Published in final edited form as:
J Phys Chem B. 2009 May 14; 113(19): 6692–6702. doi:10.1021/jp9016773.

Probing the effect of amino-terminal truncation for $A\beta_{1-40}$ peptides

Takako Takeda and **Dmitri K. Klimov***
Department of Bioinformatics and Computational Biology, George Mason University, Manassas, VA 20110

Abstract

We examine the effect of deletion of the amino-terminal (residues 1 to 9) on the structure and energetics of $A\beta_{1-40}$ peptides. To this end, we use replica exchange molecular dynamics to compare the conformational ensembles of $A\beta_{1-40}$ and amino-truncated $A\beta_{10-40}$ monomers and dimers. Overall, the deletion of the amino-terminal appears to cause minor structural and energetic changes in Aβ monomers and dimers. More specifically, our findings are as follows: (1) There is a small but discernible conversion of β-strand structure into helix upon amino-terminal deletion; (2) Secondary structure changes due to truncation are caused by missing side chain interactions formed by the amino-terminal; (3) The amino-terminal together with the central sequence region (residues 10–23) represents the primary aggregation interface in $A\beta_{1-40}$ dimers. The amino-truncated $A\beta_{10-40}$ retains this aggregation interface, which is reduced to the central sequence region. We argue that the analysis of available experimental data supports our conclusions. Our findings also suggest that amino-truncated $A\beta_{10-40}$ peptide is an adequate model for studying $A\beta_{1-40}$ aggregation.

Introduction

Currently accepted view postulates that the onset of Alzheimer's disease is associated with the extracellular aggregation of Aβ peptides that involves oligomerization of individual Aβ chains and formation of amyloid fibrils.[1,2] Although Aβ amyloid fibrils show cytotoxic properties,[3] it is believed that Aβ oligomers are the primary cytotoxic species.[4–6] Recently, it has been shown that synaptic structure and function can be impaired even by the smallest Aβ oligomers, dimers.[7] Aβ peptides are produced by natural cleavage of the transmembrane amyloid precursor protein. They are released in a variety of lengths and, while the 40- or 42-residue species, $A\beta_{1-40}$ and $A\beta_{1-42}$, are the most common, other peptide fragments are also naturally present. Among them are amino-truncated species $A\beta_{x-40}$ and $A\beta_{x-42}$, where x is the first amino acid retained in the peptide fragment.[8,9] In particular, the peptides with x = 3,5,8,9,11 were reported. Importantly, it has been estimated that the amino-truncated species may constitute up to 60% of all Aβ aggregated peptides.[8]

In the past the impact of C-terminal truncation on Aβ amyloid formation has attracted significant experimental and computational attention, in part, because Aβ species, $A\beta_{1-39}$, $A\beta_{1-40}$, and $A\beta_{1-42}$, are the main constituents of Aβ fibrils.[10] It is well established that $A\beta_{1-42}$ peptides are considerably more amyloidogenic than $A\beta_{1-40}$ and are capable of aggregating without detectable lag time.[11] It is also known that compared to $A\beta_{1-40}$ peptides two additional amino acids in $A\beta_{1-42}$ induce noticeable shift towards higher order oligomer assemblies.[12] Furthermore, single site mutagenesis at the positions 19–23 leads to different changes in the $A\beta_{1-40}$ and $A\beta_{1-42}$ oligomerization.[13] These findings suggest that $A\beta_{1-40}$ and $A\beta_{1-42}$ aggregate via different pathways.

E-mail: dklimov@gmu.edu.

In comparison with the C-terminal, the role of the N-terminal in Aβ aggregation has been less studied and is not well understood.[14] Several lines of experimental evidence suggest that in $A\beta_{1–40}$ fibrils roughly ten N-terminal residues form disordered structure.[15–18] Consequently, it is conceivable that the N-terminal is not important for fibril formation. Indeed, recent solid-state NMR studies did show that $A\beta_{1–40}$ and the truncated species $A\beta_{10–40}$ form very similar fibril structures.[17,19] Apparently minor role of the N-terminal in fibril assembly does not imply that it is also irrelevant in earlier stages of aggregation. Biophysical studies have revealed that progressive deletions of amino acids from the N-terminal (x = 1,4,8) affect the amount of Aβ deposits and their cytotoxicity.[20] On the other hand, the size distributions of $A\beta_{x–40}$ oligomers with x from 1 to 10 remain qualitatively similar and mostly include Aβ species from monomers to tetramers.[13] These observations raise the question on the exact role, which the N-terminal plays in Aβ aggregation.

In silico studies, such as molecular dynamics (MD) simulations, can probe Aβ aggregation on a molecular level.21 In recent years several MD studies have explored the conformational properties of Aβ monomers and dimers.22–26 In particular, explicit water replica exchange molecular dynamics (REMD) simulations have found several structured regions in generally disordered Aβ monomer.23 Implicit solvent REMD also pointed out to generally random coil-like structure of Aβ monomer.25 In our REMD simulations of Aβ monomers and dimers we used N-terminal truncated peptide $A\beta_{10–40}$.[27] We have showed that, although random coil dominates $A\beta_{10–40}$ conformational ensemble, significant populations of helix and β structure are also present. In particular, helix is most frequently formed in the sequence region 14–21 of $A\beta_{10–40}$ monomer, but is gradually replaced with β-strand conformers in $A\beta_{10–40}$ dimers and higher order aggregates. Furthermore, our simulations demonstrated that the primary aggregation interface in $A\beta_{10–40}$ dimers involves the sequence region 10–23, whereas the C-terminal was predicted to play minor role.[27] However, it is not *a priori* clear if these conformational properties and aggregation scenarios are applicable to full-length $A\beta_{1–40}$ peptides.

To answer the questions posed above we performed REMD simulations of $A\beta_{1–40}$ monomers and dimers and compared their structures and aggregation properties with those of $A\beta_{10–40}$.[27] We show that the deletion of the residues 1 to 9 in $A\beta_{1–40}$ does not qualitatively change the distribution of structures sampled by the monomer nor the aggregation interface in the dimer. However, the removal of the N-terminal does increase the helical propensity in Aβ monomers and dimers, while simultaneously reducing the fraction of β-structure. The analysis of REMD simulations indicate that these secondary structure changes are due to missing side chain interactions formed by the N-terminal with the central and C-terminal regions of Aβ peptides.

Model and Simulation Methods

Molecular dynamics simulations

To perform simulations of Aβ peptides we used CHARMM MD program[28] and all-atom force field CHARMM19 coupled with the SASA implicit solvent model.[29] The CHARMM19 +SASA force field is not known for bias toward particular protein secondary structure. It has been used to fold polypeptides, which contain α-helices or β-sheets.[30,31] CHARMM19+SASA simulations were also employed for studying oligomerization of amyloidogenic peptides.[32,33]

In this work, we use two versions of Aβ peptide - the full length wild-type $A\beta_{1–40}$ and the amino-truncated $A\beta_{10–40}$, in which nine N-terminal residues are removed (Fig. 1). To analyze monomeric peptide folding and aggregation we consider monomers and dimers of $A\beta_{1–40}$ and $A\beta_{10–40}$. The properties of $A\beta_{10–40}$ monomers and dimers were investigated in our previous study.[27] Here, by performing new simulations of $A\beta_{1–40}$ monomers and dimers and comparing

them with those for $A\beta_{10–40}$ we evaluate the role of the N-terminal residues 1–9 in the ensemble of structures sampled by $A\beta_{1–40}$.

Replica exchange simulations

To achieve exhaustive conformational sampling we used replica exchange molecular dynamics (REMD).[34] This method provides efficient sampling of rugged free energy landscapes governing protein folding and aggregation.[26,32,33,35–39] To simulate $A\beta_{1–40}$ monomers and dimers we used 24 replicas distributed linearly in the temperature range from 300 to 530K. The exchanges were attempted every 80 ps in all neighboring replica pairs. The average acceptance rates were 62% (monomer) and 47% (dimer). In all, we produced four (monomer) and eight (dimer) REMD trajectories of the length 0.8μ*s* each (per replica). Therefore, the cumulative simulation time for all replicas was about 76μ*s* (monomer) and 152μ*s* (dimer). The structures were saved every 40 ps. Between replica exchanges the system was evolved using NVT under-damped Langevin dynamics with the damping coefficient $\gamma = 0.15ps^{-1}$ and the integration step of 2*fs*. The initial equilibration intervals τ_{eq} were determined by monitoring the effective energy E_{eff}, which is the sum of potential and solvation energies. Consequently, the initial parts of REMD trajectories of the lengths up to 100 ns were excluded and the cumulative equilibrium simulation times were reduced to τ_{sim} = 66μ*s* (monomer) and 128μ*s* (dimer). Aβ systems were subject to spherical boundary condition with the radius R_s=90Åand the force constant $k_s = 10kcal/(molÅ^2)$. For dimers the concentration of Aβ peptides was of an order of *mM*.

Computation of structural probes

To characterize intra- and interpeptide interactions we computed the number of side chain contacts. A contact is formed, if the distance between the centers of mass of side chains is less than 6.5Å. This cut-off approximately corresponds to the onset of hydration of side chains as the separation distance between them increases. Backbone hydrogen bonds (HBs) between NH and CO groups were assigned according to Kabsch and Sander.40 Secondary structure in Aβ peptides was determined by evaluating their dihedral angles (ϕ, ψ).[41,42] To this end, the grid with the spacing of 18° was superimposed on the Ramachandran plot. The β-strand conformations are enclosed by the vertices of the polygon (−180°,180°), (−180°,126°), (−162°, 126°), (−162°,108°), (−144°,108°), (−144°,90°), (−50°,90°), (−50°,180°); helix structures are confined to the polygon (−90°,0°), (−90°,−54°), (−72°,−54°), (−72°,−72°), (−36°,−72°), (−36°, −18°), (−54°,−18°), (−54°,0°). (Note that these definitions do not distinguish α-helix, 3_{10}-helix, or π-helix.) Using these definitions the fractions of residues in helix and β-strand conformations, *H* and *S*, can be computed in any structure. As an alternative it is possible to use the program STRIDE for secondary structure assignment.43 However, we showed in our previous study[27] that, because STRIDE defines β-structure using HBs, it may underestimate the formation of extended β-like conformations in disordered systems such as Aβ dimers and monomers. Consequently, in this work we assign secondary structure using (ϕ, ψ) angles.

Throughout the paper angular brackets < .. > indicate thermodynamic averages. Because Aβ dimers include two indistinguishable peptides, we report averages over two peptides. The distributions of states produced by REMD were analyzed using multiple histogram method.[44]

Cluster analysis of Aβ monomers

In order to probe the conformational ensemble sampled by $A\beta_{1–40}$ monomers we applied cluster analysis. Because the details of this method can be found elsewhere,[45] we present here only its short outline. We used 7000 $A\beta_{1–40}$ structures collected with the period of five REMD steps from the equilibrated REMD simulations at 360*K*. Because successive structures are, on an average, separated by several replica exchanges, they are statistically independent. Aβ conformations were clustered based on the distribution of side chain contacts. To this end, a

structure k was represented by a vector $\vec{D}(k)$ with 780 binary components, each given by the element of the contact map $C_m(i, j)$. If the residues i and j ($j>i+1$) form a contact, then $C_m(i, j) = 1$, and $C_m(i, j) = 0$, otherwise. The vector $\vec{D}_{cl}$ representing the cluster is computed as the average of the vectors $\vec{D}(k)$, where k are the indeces of structures assigned to the cluster. The peptide structural clusters were defined with the cut-off radius $R_c = 7.3$, which is equal to the maximum Euclidian distance between the cluster and a structure. To select R_c we scan its values in the range from 5 to 15. Small R_c lead to the appearance of numerous structurally similar clusters, whereas large R_c result in merging structurally distinct clusters.

Convergence of REMD simulations

To evaluate the quality of REMD sampling we consider the number N_s of the unique states (E_{eff},N_d), which were sampled in the course of $A\beta_{1–40}$ dimer simulations at least once. Each state (E_{eff} ,N_d) is defined by the effective energy E_{eff} and the number of interpeptide HBs, N_d. Fig. 2 shows N_s for $A\beta_{1–40}$ dimer as a function of the cumulative equilibrium simulation time τ_{sim}. At $\tau_{sim} \gtrsim 80\mu s$ N_s approximately levels off suggesting convergence of REMD. To further test the reliability of REMD we divided the $A\beta_{1–40}$ dimer simulations into two equal subsets and analyzed them independently. The thermodynamic quantities from the two subsets differed by no more than 6% (with respect to the numbers of HBs and side chain contacts) or 2% (with respect to secondary structure fractions). The errors for $A\beta_{1–40}$ monomers are smaller than those for the dimers. The error analysis for $A\beta_{10–40}$ monomers and dimers was reported earlier.[27]

Testing the reliability of implicit solvent model

To test the implicit solvent model used in our study we computed the chemical shifts $\delta_{sim}(i)$ using the REMD sampling of $A\beta_{1–40}$ monomer and the program SHIFTS.[46] We choose to analyze C_α and C_β chemical shifts because of their sensitivity to α-helix and β-strand structures.[47] Fig. 3 shows the comparison of $\delta_{sim}(i)$ with the corresponding experimental chemical shifts $\delta_{exp}(i)$ measured by Zagorski and coworkers for $A\beta_{1–40}$-Met^{red} monomers at 278K.[47] It is seen that the C_β experimental and simulation chemical shifts are in perfect agreement (the correlation factor 0.999). The consistency of C_α $\delta_{sim}(i)$ and $\delta_{exp}(i)$ is also reasonably good (the correlation factor of 0.987). Some discrepancy between $\delta_{sim}(i)$ and $\delta_{exp}(i)$ for the residues 4–7 and 12–20 suggests that our simulations somewhat overestimate the helix fraction for these residues.[27,48] However, the overall agreement of the experimental and *in silico* distributions of chemical shifts suggests that the implicit solvent model reproduces the conformational ensemble of $A\beta_{1–40}$ monomers.

Results

Using REMD we investigated the distribution of structures sampled by $A\beta_{1–40}$ monomers and dimers (Fig. 1). We have previously showed that the amino-truncated $A\beta_{10–40}$ peptides dock to amyloid fibrils and assume ordered β-sheet conformations at the locking temperature $T_l \approx 360K$.[33] Consequently, we report the structural properties of $A\beta_{1–40}$ monomers and dimers and compare them with those of $A\beta_{10–40}$ at the temperature 360K. The REMD simulations of $A\beta_{10–40}$ were published by us earlier.[27] Following the allocation of β-structure in $A\beta_{1–40}$ amyloid fibril,[17] we distinguish three sequence regions in $A\beta_{1–40}$ - the N-terminal (residues 1 to 9, denoted as NT); the central region (residues 10 to 23, CR), which corresponds to the first fibril β-strand; and the C-terminal (residues 29 to 39, CT), which corresponds to the second fibril β-strand (Fig. 1). In what follows the changes in $A\beta_{1–40}$ secondary structure or free energy refer to the differences with respect to the truncated peptide $A\beta_{10–40}$.

Comparison of $A\beta_{1-40}$ and $A\beta_{10-40}$ secondary structure

Using the REMD sampling we computed the distribution of secondary structure as described in Model and Simulation Methods. On an average, the fractions of residues in the β-strand and helix conformations in $A\beta_{1-40}$ monomer are $< S >= 0.30$ and $< H >= 0.27$. Fig. 4a shows the fractions of helix $< H(i) >$ and β-strand $< S(i) >$ structure formed by individual residues i in $A\beta_{1-40}$ monomer. It is seen that the helical conformations tend to localize in the central region CR (residues 14–21), in which the average helical fraction is $< H(CR) >= 0.43$. Elsewhere in $A\beta_{1-40}$ monomer the helical structure is less frequent (in the NT region, $< H(NT) >= 0.25$; in the CT, $< H(CT) >= 0.12$). The β-strand conformations are frequently observed in the NT ($< S(NT) > = 0.32$) and CT ($< S(CT) >= 0.34$) regions, but are less probable in the CR ($< S(CR) >= 0.23$).

Compared to $A\beta_{10-40}$ monomer the fraction of β-strand structure in $A\beta_{1-40}$ is increased by $<\Delta S>=<S>A\beta_{1-40} - <S>A\beta_{10-40} =0.06$ (from 0.24 to 0.30), while the helix fraction is decreased by $<\Delta H>=<H>A\beta_{1-40} - <H>A\beta_{10-40} =-0.05$ (from 032 to 0.27). Fig. 4b demonstrates the changes in secondary structure, which occur in $A\beta_{1-40}$ monomer compared to $A\beta_{10-40}$, $<\Delta S(i)>=<S(i)>A\beta_{1-40} - <S(i)>A\beta_{10-40}$ and $<\Delta H(i)>=<H(i)>A\beta_{1-40} - <H(i)>A\beta_{10-40}$. The largest decrease in helical population $< \Delta H(CR) >= -0.08$ occurs in the CR region, whereas in the CT it is smaller ($< \Delta H(CT) >= -0.03$). In contrast, the increase in β-structure fraction is spread throughout $A\beta_{1-40}$ monomer ($< \Delta S(CR) >= 0.06$ and $< \Delta S(CT) >= 0.05$). Overall, the largest increase in $< S(i) >$ occurs at the positions 14–23,26,27,30,31,34,35,39, whereas the largest decrease in $< H(i) >$ is seen at 12–18,23,26,27,30,34,35. Two further observations follow from Fig. 4b. First, the secondary structure changes $< \Delta S(i) >$ and $< \Delta H(i) >$ are anticorrelated (the correlation coefficient is −0.6). Second and, more importantly, the window-averaged profiles of $< \Delta S(i) >$ and, to a lesser degree, of $< \Delta H(i) >$ suggest that the changes in secondary structure caused by the inclusion of the NT are not localized within the CR region, but extend over entire $A\beta_{1-40}$ sequence.

The structural changes in $A\beta_{1-40}$ dimer are similar to those observed for the monomer. The fraction of β-structure $< S >$ is increased from 0.37 ($A\beta_{10-40}$) to 0.40 ($A\beta_{1-40}$, $< \Delta S >= 0.03$), while the corresponding decrease in helical fraction is from 0.21 to 0.18 ($< \Delta H >= -0.03$). As a result, the amount of β-structure in $A\beta_{1-40}$ dimer exceeds that of helix by a factor of 2. The changes in secondary structure for individual residues are shown in Fig. 4c. The largest changes $< \Delta S(i) >$ and $< \Delta H(i) >$ are observed in the CR region, where $< \Delta S(CR) >= 0.05$ and $< \Delta H(CR) >= -0.06$. In contrast, the secondary structure changes in the CT region are minor ($< \Delta S(CT) >= 0.01$ and $< \Delta H(CR) >\approx 0.0$). As in Aβ monomers the changes in β-strand and helix structure are anticorrelated (the correlation coefficient is −0.8). Consequently, there appears to be a direct interconversion of helix and β-strand structures, which bypasses the random coil conformations.

The analysis of the secondary structure in Aβ dimers suggests that the changes tend to localize in the CR region adjacent to the NT, while being relatively weak in the CT region, which is separated from the NT by 20 amino acids. This finding contrasts that seen in Aβ monomer, in which changes in secondary structure are spread across the entire $A\beta_{1-40}$ sequence (compare (b) and (c) in Fig. 4).

Distribution of intrapeptide interactions in $A\beta_{1-40}$

One may expect that the differences in conformational ensembles sampled by $A\beta_{1-40}$ and $A\beta_{10-40}$ are related to the interactions formed by the NT. To explore this possibility we computed the thermal map $< C_m(i, j) >$ of contacts formed between the residues i and j in $A\beta_{1-40}$ monomer (Fig. 5a). This figure shows that a large fraction of contacts are local ($|i-j| \leq 6$). From the contact map it follows that the total number of side chain contacts is $< C_m >=$

48.9 and about 56% of them falls into the local category. It is also clear that the NT region forms long range interactions with the CR and CT regions. Indeed, the thermal probability of the NT to form long range ($|i-j| > 6$) side chain contacts with the 10–40 sequence fragment is 0.97. To directly assess the role of the NT interactions in $A\beta_{1-40}$ monomer we plot in Fig. 5b the number of contacts formed by the NT with the residues $10 \leq i \leq 40$, $< K_m(i) >$. The total number of contacts formed between the NT and the residues 10–40 is $< K_m >= 15.1$. Because most of the side chain contacts in $A\beta_{1-40}$ monomer are local, the largest values of $< K_m(i) >$ are observed within the CR region, although significant number of contacts is also formed with the CT. Specifically, from Fig. 5b we compute that the overall number of contacts, which the NT forms with the CR and CT, are $< K_m(CR) >= 7.8$ and $< K_m(CT) >= 5.0$, respectively. In contrast, it follows from Fig. 5b that the number of hydrogen bonds (HB) between the NT and the residues 10–40 $< N_m >$ is only 2.7.

Fig. 5b also compares the intrapeptide interactions formed by the NT in $A\beta_{1-40}$ monomers and dimers. The number of intrapeptide contacts formed by the NT with the residues $10 \leq i \leq 40$ in the dimer, $< K_d(i) >$, is similar to $< K_m(i) >$ in the CR region, but is noticeably smaller in the CT. In fact, the overall numbers of contacts, which the NT forms with the CR and CT regions in the dimer, are $< K_d(CR) >= 7.2$ and $< K_d(CT) >= 2.8$, respectively. The total number of intrapeptide contacts between NT and the residues 10–40 in the dimer is $< K_d >= 11.8$. As for $A\beta_{1-40}$ monomer the total number of intrapeptide HBs between the NT and the residues 10–40 in the dimer $< N_d >$ is small (2.6).

Effect of $A\beta_{1-40}$ amino-terminal deletion on the free energy landscape

To further assess the impact of the NT region we used REMD simulations to compute the free energy contour plot $\Delta F(S,H)$ for $A\beta_{1-40}$ monomer as a function of β-strand S and helix H fractions. Fig. 6a shows that compared to $A\beta_{10-40}$ monomer the $A\beta_{1-40}$ free energy basin becomes broader and shifts from the region of $H \sim 0.35$ and $S \sim 0.2$ to $H \sim 0.25$ and $S \sim 0.3$. This shift in free energy is consistent with the changes in the strand and helix populations, $< \Delta S >$ and $< \Delta H >$, described above. To provide a quantitative estimate of free energy change we plot in Fig. 6b the free energies of $A\beta_{10-40}$ and $A\beta_{1-40}$ monomers as a function of S. Addition of nine amino-terminal residues to $A\beta_{10-40}$ decreases the free energy of β-structure by $\Delta\Delta F_S = \Delta F_S(A\beta_{1-40}) - \Delta F_S(A\beta_{10-40}) = -1.9RT$ and shifts its minimum from $S \sim 0.17$ to ~ 0.27. Difference in free energy of the helix structure is less than RT. The changes in free energy landscape for $A\beta_{1-40}$ dimers are similar to those for the monomers. For example, the free energy minimum of the β-structure in the dimer deepens by $\Delta\Delta F_S = -1.6RT$ (data not shown). Therefore, the NT region in $A\beta_{1-40}$ appears to stabilize β-structure by decreasing its free energy.

$A\beta_{1-40}$ aggregation interface

To probe the aggregation interface in $A\beta_{1-40}$ dimer, we used REMD simulations to compute the thermal map $< C_d(i, j) >$ of interpeptide contacts between the residues i and j. Fig. 7a shows that the distribution of interpeptide contacts is highly uneven. Most frequently, they are formed by the NT and CR regions, whereas the CT is relatively rarely involved in dimer formation (as illustrated in Fig. 1b). From Fig. 7a we compute that the numbers of interpeptide side chain contacts formed by the NT, CR, and CT regions are $< C_d(NT) >= 15.1$, $< C_d(CR) >= 16.8$, $< C_d(CT) >= 9.0$ or 1.7, 1.2, and 0.8 per residue, respectively. The total number of interpeptide contacts is $< C_d >= 46.9$. More detailed description of the aggregation interface can be inferred from the Table 1a. The largest number of interpeptide contacts is formed between the CR regions followed by the NT-CR and NT-NT interactions. The least frequent contacts are formed by the CT regions.

To probe the orientation of $A\beta_{1–40}$ peptides in the dimer we considered the vectors $\vec{R}(k) = \vec{r}_{C_\alpha}(23, k) - \vec{r}_{C_\alpha}(10, k)$, where $\vec{r}_{C_\alpha}(23, k)$ and $\vec{r}_{C_\alpha}(10, k)$ are the radius-vectors of C_α atoms of the residues Asp23 and Tyr10 in the peptide k(=1,2). By definition, $\vec{R}(k)$ describes the orientation of the CR region. This region was selected, because the fraction of ordered structure (helix or strand) in the CR is high (~ 0.7) and, consequently, this region is relatively rigid. More importantly, the CR forms the largest number of contacts $< C_d (CR) >$ in the aggregation interface. Fig. 7b displays the distribution $P(\cos\phi)$, where ϕ is the angle between $\vec{R}(1)$ and $\vec{R}(2)$ The distribution $P(\cos\phi)$, which is weakly bimodal, shows a slight preference of $A\beta_{1–40}$ peptides to form antiparallel aggregation interface. The probability of antiparallel orientation (i.e, of $\cos\phi < 0$) is 0.53.

The $A\beta_{1–40}$ aggregation interface emerging from Fig. 7a can be compared with that for $A\beta_{10–40}$ dimer.[27] At $T = 360K$ used in this study the numbers of interpeptide side chain contacts formed by the CR and CT $A\beta_{10–40}$ regions are $< C_d(CR) >= 16.1$ and $< C_d(CT) >= 8.6$ or 1.2 and 0.8 per residue, respectively. Table 1b shows that most of interpeptide contacts are formed between the CR regions, whereas the contacts between CT terminals are almost four-fold less frequent. We also note that $A\beta_{10–40}$ dimer forms an antiparallel aggregation interface with almost the same probability (0.60)[27] as reported above for $A\beta_{1–40}$.

We have also computed the thermal distribution of interpeptide HBs for $A\beta_{1–40}$ dimers (data not shown). The numbers of HBs formed by the NT, CR, and CT regions are 2.5, 2.3, and 1.5, respectively. The largest number of interpeptide HBs are formed between the NT regions (0.9) followed by those formed between the NT and CR (0.7) and between the CR regions (0.7). The smallest number of HBs is formed between the CTs (0.3). The total number of interpeptide HBs in $A\beta_{1–40}$ dimer is 7.0. Two conclusions can be drawn from these computations. First, the distribution of interpeptide HBs is qualitatively similar to that of side chain contacts. Second, backbone HBs appear to play minor role in the dimer aggregation interface as the number of side chain contacts exceeds that of HBs by about a factor of seven.

Discussion

$A\beta_{1–40}$ and $A\beta_{10–40}$ peptides have similar conformational ensembles

In this study we investigated the impact of the amino-terminal on the conformational ensembles of Aβ peptides. The role of the NT region was inferred from the comparison of the secondary structure, interactions, and free energy landscapes of full-length $A\beta_{1–40}$ and amino-truncated $A\beta_{10–40}$ peptides. We showed that compared to $A\beta_{10–40}$ the fraction of β-structure in $A\beta_{1–40}$ monomer increases 25% ($< \Delta S >= 0.06$), whereas the helix fraction decreases about 16% ($< \Delta H >= -0.05$). These structural changes are consistent with those observed in the free energy landscape (Fig. 6).

With respect to $A\beta_{10–40}$ the secondary structure changes in $A\beta_{1–40}$ monomer occur in both the CR and CT regions (Fig. 4b). For example, the β fractions in the CR and CT increase 35% ($< \Delta S(CR) >= 0.06$) and 17% ($< \Delta S(CT) >= 0.05$), respectively. The helix fractions in the CR and CT decrease 16% ($< \Delta H(CR) >= -0.08$) and 20% ($< \Delta H(CT) >= -0.03$), respectively. In $A\beta_{1–40}$ dimers the inclusion of the NT also enhances β-strand structure (by 8% or $< \Delta S >= 0.03$) and reduces the probability of helix conformers (by 14% or $< \Delta H >= -0.03$). However, these changes mainly occur near the NT (Fig. 4c). Within the CR region the β-strand fraction increases 14% ($< \Delta S(CR) >= 0.05$), while the helix fraction decreases 19% ($< \Delta H(CR) >= -0.06$). In contrast, in the CT region the changes in helix and β-strand fractions are negligible (less than 3% or ≤ 0.01).

The changes in secondary structure can be rationalized by considering the number of contacts formed by the NT with the residues $10 \leq i \leq 40$ in $A\beta_{1–40}$ monomer and dimer. In the monomer

the NT forms with the CT about two-thirds of the contacts which it forms with the CR (< $K_m(CT)$ >= 5.0 vs < $K_m(CR)$ >= 7.8). However, in $A\beta_{1–40}$ dimer the NT forms with the CT only one-third of the contacts which it forms, on an average, with the CR (< $K_d(CT)$ >= 2.8 vs < $K_d(CR)$ >= 7.2). By comparing the changes in the secondary structure and the distribution of intrapeptide contacts one may suggest the two are related. Because the NT in $A\beta_{1–40}$ monomer forms large number of contacts with both the CR and CT regions, the changes in secondary structure propagate the entire Aβ sequence (data above and Fig. 4b and Fig. 5b). In contrast, in $A\beta_{1–40}$ dimer the NT tends to form most interactions with the CR region, which, in turn, experiences the largest change in secondary structure (data above and Fig. 4c and Fig. 5b). Furthermore, in $A\beta_{1–40}$ dimer the number of NT-CT contacts is twice smaller than in the monomer. Accordingly, the changes in the strand and helix fractions in the dimer CT region are negligible compared to those in the monomer CT.

To further probe the relation between the NT interactions and the changes in secondary structure, we clustered $A\beta_{1–40}$ monomer conformations as described in Model and Simulation Methods. We found that 80% of structures can be grouped into four large clusters (Table 2). The structural clusters differ with respect to the numbers of contacts between the NT and CR, $K(NT–CR)$, and between the NT and CT, $K(NT–CT)$, and with respect to the fractions of β-strand and helix in the CR ($S(CR)$ and $H(CR)$) and CT ($S(CT)$ and $H(CT)$) regions. In Table 2a the clusters are arranged in the descending order of $K(NT–CR)$, which ranges from 8.0 in CL1 to 6.7 in CL4. Importantly, the fraction of helix $H(CR)$ monotonically increases from 0.41 (CL1) to 0.54 (CL4), while the strand fraction $S(CR)$ reveals a two-fold decrease, from 0.27 (CL1) to 0.13 (CL4). Similarly, Table 2b lists the clusters in the descending order of the number of NT-CT contacts, $K(NT–CT)$. An almost two-fold decrease in $K(NT–CT)$ from 5.8 (CL1) to 3.0 (CL4) results in two-fold monotonic increase in the helix fraction $H(CT)$, from 0.10 (CL1) to 0.20 (CL4). Simultaneously, the strand fraction shows a matching reduction from 0.37 (CL1) to 0.18 (CL4). As follows from Table 2b the formation of NT-CT contacts results in the decrease in the monomer radius of gyration from 15.4 Å(CL4) to 14.1 Å(CL2). In summary, Table 2 demonstrates that with the increasing number of contacts formed by the NT the helix fractions in the CR and CT reveal monotonic decrease, while the β-strand fractions show an almost perfect opposite trend. As illustration to cluster analysis two representative monomer conformers with formed and broken NT interactions are shown in Fig. 1a. Taken together the findings presented above suggest that the interactions of the NT with the CR and CT regions are responsible for the changes in their secondary structure.

It is important to note that the analysis of intrapeptide interactions indicates that the number of HBs formed by the NT with other sequence regions is six-fold smaller than the number of respective side chain contacts (< N_m >= 2.7 vs < K_m >= 15.1). Similar result is obtained for Aβ dimer. Thus, it appears that the secondary structure changes in Aβ are driven mostly by side chain interactions rather than backbone HBs.

As a result of the NT interactions, the β-content in $A\beta_{1–40}$ monomers exceeds the helical one (0.30 vs 0.27), but most of $A\beta_{1–40}$ residues still adopt disordered random coil conformations (their fraction is 0.43). (For comparison, in the $A\beta_{10–40}$ monomer the fractions of strand, helix, and coil structures are 0.24, 0.32, 0.44 at 360*K*, respectively.27) The distribution of $A\beta_{1–40}$ secondary structure obtained by us is consistent with previous experimental and simulation studies, which did not identify a stable native fold in Aβ monomer.[23,25,47]

In summary, we traced the differences in the structural ensembles of $A\beta_{1–40}$ and $A\beta_{10–40}$ to the side chain interactions formed by the amino-terminal. However, because structural changes are relatively small (not to exceed 35%) and both peptides retain overall random coil structure, we conclude that there are no qualitative differences in the conformational ensembles sampled by $A\beta_{1–40}$ and $A\beta_{10–40}$. This conclusion finds support in the comparison of chemical shifts

computed from simulations[27] and obtained experimentally.[47] In our previous simulations of $A\beta_{10–40}$ we computed the chemical shifts for C_α and C_β atoms and showed that are in good agreement with the experimental shifts measured by Zagorski and coworkers for $A\beta_{1–40}$ monomer.[47] This result implies that the truncation of the amino-terminal from $A\beta_{1–40}$ does not lead to qualitative changes in the structural properties of the peptide. In other words, the conformational ensembles of $A\beta_{10–40}$ and $A\beta_{1–40}$ appear to be qualitatively similar. Because the overall structural changes in the dimer are smaller than in the monomer and tend to affect the sequence region adjacent to the NT, we propose that in higher order oligomers the impact of the NT deletion should further diminish.

$A\beta_{1–40}$ and $A\beta_{10–40}$ peptides have similar aggregation interfaces

Using REMD simulations we mapped the aggregation interface in $A\beta_{1–40}$ dimer. The results suggest that the aggregation interface primarily involves the NT and CR regions, whereas the CT is relatively rarely engaged in dimer formation. For example, the number of interpeptide contacts per residue formed by the NT region is twice larger than that for the CT (1.7 vs 0.8). Similarly, the number of interpeptide contacts per residue in the CR is 50% more than in the CT (1.2 vs 0.8). Table 1a also shows that the number of interpeptide contacts between the CR regions exceeds that between the CTs by a factor of 3. Qualitatively similar distribution of interpeptide interactions is obtained for $A\beta_{10–40}$ dimer,[27] for which the number of contacts (per residue) formed by the CR regions is larger than that formed by the CTs 50%. Table 1b also shows that the CT-CT contacts are almost four-fold less frequent than those between the CRs.

To provide direct comparison of the involvement of the 10–40 fragment in aggregation, we included in Table 1 the fractions of contacts computed with respect to the total number of interpeptide contacts formed by the CR and CT regions in the 10–40 dimer fragment, $<C_d(CR+CT)>$. In $A\beta_{1–40}$ and $A\beta_{10–40}$ dimers $<C_d(CR+CT)>$ are 15.3 and 20.2, respectively. Table 1 shows that these contact fractions are remarkably similar for $A\beta_{1–40}$ and $A\beta_{10–40}$. These findings indicate that the distributions of contacts along the sequence and between sequence regions in $A\beta_{1–40}$ and $A\beta_{10–40}$ dimers are similar. In both cases, most interpeptide contacts are formed by the aminoterminal regions - the NT and CR regions in $A\beta_{1–40}$ and the CR region in $A\beta_{10–40}$. Additionally, both $A\beta_{1–40}$ and $A\beta_{10–40}$ dimers show a tendency to form antiparallel aggregation interface (Fig. 7b). Consequently, we surmise that the deletion of the amino-terminal in $A\beta_{1–40}$ does not qualitatively change the aggregation interface in Aβ dimers.

It is important to compare our results with those obtained by Caflisch and coworkers.[49] These authors explored the aggregation profile along $A\beta_{1–42}$ sequence using seven- and 11-mer overlapping fragments of this peptide and performing MD simulations of oligomer assembly. An aggregationprone region was identified as 12–22 with other sequence regions revealing much lower aggregation propensity. Qualitatively similar suggestion was recently put forward by Derreumaux and coworkers.[50] These reports are consistent with our findings that the CT region may not represent the primary aggregation interface.

Comparison with experimental data

It is important to compare our computational predictions with available experimental data. There are indications that the NT region plays a minor role in Aβ fibril structure. Solid-state NMR, paramagnetic resonance, and electron cryomicroscopy studies revealed that the NT region in $A\beta_{1–40}$ fibril is disordered.[16–18] Proteolysis experiments also suggested that the NT region in $A\beta_{1–40}$ fibril is exposed to solvent and is not buried in the fibril core.[15] Furthermore, solid-state NMR studies of $A\beta_{1–40}$ and the amino-truncated $A\beta_{10–40}$ showed that both form very similar fibril structures.[17,19] It is worth noting that the fibril structure for $A\beta_{1–42}$ peptide also reveals disordered N-terminal region (residues 1 to 17).[51]

However, the NT region does affect, at least to some extent, the $A\beta_{1–40}$ aggregation pathway.[20] It was found that the amino-truncated $A\beta_{8–40}$ demonstrates enhanced aggregation as its sedimentation increases about 50% within 7 days compared to $A\beta_{1–40}$. An opposite trend was observed for $A\beta_{4–40}$, for which the amount of sediments decreases roughly in half. Similar conclusions follow from the experimental study, which investigated the aggregation of several Aβ mutants.[52] While the wild-type $A\beta_{1–40}$ aggregates with the average lag time $t_{l,0} = 4.8h$, the mutant A2T shows no discernible time lag upon aggregation ($t_l = 0$). An opposite trend is reported for the mutant H6R, for which t_l is increased two-fold. Interestingly, the changes in t_l caused by the NT mutations are comparable with those seen for well-studied E22G ("Arctic", $t_l = 0$) or D23N ("Iowa", $t_l \approx 1.4t_{l,0}$) mutants.

The involvement of the NT region in aggregation has been demonstrated by photo-induced cross-linking experiments on Aβ wild-type and amino truncated oligomers.[13] The $A\beta_{1–40}$ oligomer size distribution predominantly shows monomer, dimer, trimer, and tetramer species. Similar distributions were observed for $A\beta_{x–40}$ oligomers with $x = 3$ and 5, although minor subpopulations of higher order oligomers did emerge. The distribution for $A\beta_{10–40}$ reveals a shift to smaller oligomers (monomers to trimers) due to partial depletion of the tetramer and higher order oligomer populations. Dramatic changes in the oligomer size distribution occur only with the deletion of Tyr10 ($x = 11$), for which no species larger than dimers are observed. The comparison of the deletions of N- and C-terminal amino acids demonstrates that the length of the C-terminal rather than of the N-terminal exerts the largest effect on oligomerization pathway.[13]

Taken together the experimental studies mentioned above indicate that the NT region is involved in $A\beta_{1–40}$ aggregation. These results are consistent with our current findings suggesting that $A\beta_{1–40}$ aggregates primarily using its amino-terminal and central sequence region (Fig. 7a and Table 1a). However, the experimental oligomer size distribution seems to suggest that the removal of the NT region (residues 1 to 9) does not qualitatively change the aggregation pathway. [13] This observation also agrees well with our conclusion that the aggregation interfaces in $A\beta_{1–40}$ and $A\beta_{10–40}$ dimers are similar (Table 1). As follows from our simulations the dimer assembly is mainly driven by side chain interactions rather than by backbone HBs. This observation is consistent with those made for other amyloidogenic peptides. It has been shown using explicit water MD that initial stages in oligomerization of the peptide NFGAIL primarily involve side chain interactions.[53]

Finally, our REMD simulations show that the interactions formed by the NT region introduce a small but discernible bias toward β-structure in $A\beta_{1–40}$ conformational ensemble as revealed by the computations of secondary structure and free energy landscapes. Currently, we are not aware of secondary structure studies of amino-truncated $A\beta_{x–40}$ peptides. However, our observations are consistent with the CD measurements, which have been performed on the aggregated fragments $A\beta_{x–42}$ and compared with the data for the full-length $A\beta_{1–42}$.[20] It was found that the aggregated assemblies of full-length and truncated peptides are dominated by β-structure and no qualitative secondary structure differences between them have been detected.

Conclusions

We examined the effect of the deletion of the amino-terminal (residues 1 to 9) on the structure and energetics of $A\beta_{1–40}$ peptides. Using REMD simulations and comparing the conformational ensembles for the full length $A\beta_{1–40}$ and amino-truncated $A\beta_{10–40}$ monomers and dimers we arrived at the following conclusions: (1) There is a small but discernible conversion of β-strand structure into helix upon amino-terminal deletion; (2) The secondary structure changes due to amino-terminal truncation are caused by missing side chain

interactions formed by the aminoterminal; (3) The amino-terminal together with the central sequence region (residues 10–23) represents the primary aggregation interface in $A\beta_{1–40}$ dimers. Strikingly, the amino-truncated peptide $A\beta_{10–40}$ retains this aggregation interface, which is reduced to central sequence region. Overall, the deletion of the amino-terminal in $A\beta_{1–40}$ monomers and dimers causes relatively minor structural and energetic changes. The analysis of available experimental data appears to support this conclusion. Based on our findings and on the studies of Aβ fibril structures[17,19] we suggest that amino-truncated $A\beta_{10–40}$ peptide represents an adequate model for studying $A\beta_{1–40}$ aggregation.

Acknowledgments

This work was supported by the grant R01 AG028191 from the National Institute on Aging (NIH). The content is solely the responsibility of the authors and does not necessarily represent the official views of the National Institute on Aging or NIH. We thank anonymous reviewer for pointing our attention to ref.[49].

References

1. Hardy J, Selkoe DJ. Science 2002;297:353–356. [PubMed: 12130773]
2. Dobson CM. Nature 2003;426:884–890. [PubMed: 14685248]
3. Yoshiike Y, Akagi T, Takashima A. Biochemistry 2007;46:9805–9812. [PubMed: 17676931]
4. Kirkitadze MD, Bitan G, Teplow DB. J. Neurosci. Res 2002;69:567–577. [PubMed: 12210822]
5. Kayed R, Head E, Thompson JL, McIntire TM, Milton SC, Cotman CW, Glabe CG. Science 2003;300:486–489. [PubMed: 12702875]
6. Haass C, Selkoe DJ. Nature Rev. Mol. Cell. Biol 2007;8:101–112. [PubMed: 17245412]
7. Shankar GM, Li S, Mehta TH, Garcia-Munoz A, Shepardson NE, Smith I, Brett FM, Farrell MA, Rowan MJ, Lemere CA, Regan CM, Walsh DM, Sabatini BL, Selkoe DJ. Nature Medicine 2008;14:837–842.
8. Sergeant N, Bombois S, Ghestem A, Drobecq H, Kostanjevecki V, Missiaen C, Wattez A, David J-P, Vanmechelen E, Sergheraert C, Delacourte A. J. Neurochem 2003;85:1581–1591. [PubMed: 12787077]
9. Pype S, Moechars D, Dillen L, Mercken M. J. Neurochem 2003;84:602–609. [PubMed: 12558980]
10. Naslund J, Karlstrom AR, Tjernberg L, Schierhorn A, Terenius L, Nordstedt C. J. Neurochem 1996;67:294–301. [PubMed: 8667005]
11. Jarrett JT, Berger EP, Lansbury PT. Biochemistry 1993;32:4693–4697. [PubMed: 8490014]
12. Bitan G, Kirkitadze MD, Lomakin A, Vollers SS, Benedek GB, Teplow DB. Proc. Natl. Acad. Sci. USA 2003;100:330–335. [PubMed: 12506200]
13. Bitan G, Vollers SS, Teplow DB. J. Biol. Chem 2003;278:34882–34889. [PubMed: 12840029]
14. Larner AJ. Neurobiol. Aging 1999;20 65-59.
15. Kheterpal I, Williams A, Murphy C, Bledsoe B, Wetzel R. Biochemistry 2001;40:11757–11767. [PubMed: 11570876]
16. Torok M, Milton S, Kayed R, Wu P, McIntire T, Glabe CG, Langen R. J. Biol. Chem 2002;277:40810–40815. [PubMed: 12181315]
17. Petkova AT, Yau W-M, Tycko R. Biochemistry 2006;45:498–512. [PubMed: 16401079]
18. Sachse C, Fandrich M, Grigorieff N. Proc. Natl. Acad. Sci. USA 2008;105:7462–7466. [PubMed: 18483195]
19. Paravastu AK, Petkova AT, Tycko R. Biophys. J 2006;90:4618–4629. [PubMed: 16565054]
20. Pike CJ, Overman MJ, Cotman CW. J. Biol. Chem 1995;270:23895–23898. [PubMed: 7592576]
21. Ma B, Nussinov R. Curr. Opin. Struct. Biol 2006;10:445–452.
22. Xu Y, Shen J, Luo X, Zhu W, Chen K, Ma J, Jiang H. Proc. Natl. Acad. Sci. USA 2005;102:5403–5407. [PubMed: 15800039]
23. Sgourakis NG, Yan Y, McCallum SA, Wang C, Garcia AE. J. Mol. Biol 2007;368:1448–1457. [PubMed: 17397862]

24. Triguero L, Singh R, Prabhakar R. J. Phys. Chem. B 2008;112:7123–7131. [PubMed: 18476733]
25. Yang M, Teplow DB. J. Mol. Biol 2008;384:450–464. [PubMed: 18835397]
26. Jang S, Shin S. J. Phys. Chem. B 2008;112:3479–3484. [PubMed: 18303879]
27. Takeda T, Klimov DK. Proteins Struct. Funct. Bioinf. 2009 doi 10.1002/prot.22406.
28. Brooks BR, Bruccoler RE, Olafson BD, States DJ, Swaminathan S, Karplus M. J. Comp. Chem 1982;4:187–217.
29. Ferrara P, Apostolakis J, Caflisch A. Proteins Struct. Funct. Bioinform. 46 2002:24–33.
30. Ferrara P, Caflisch A. Proc. Natl. Acad. Sci. USA 2000;97:10780–10785. [PubMed: 10984515]
31. Hiltpold A, Ferrara P, Gsponer J, Caflisch A. J. Phys. Chem. B 2000;104:10080–10086.
32. Cecchini M, Rao F, Seeber M, Caflisch A. J. Chem. Phys 2004;121:10748–10756. [PubMed: 15549960]
33. Takeda T, Klimov DK. Biophys. J 2009;96:442–452. [PubMed: 19167295]
34. Sugita Y, Okamoto Y. Chem. Phys. Lett 1999;114:141–151.
35. Garcia AE, Onuchic JN. Proc. Natl. Acad. Sci. USA 2003;100 13898-13893.
36. Tsai H-H, Reches M, Tsai C-J, Gunasekaran K, Gazit E, Nussinov R. Proc. Natl. Acad. Sci. USA 2005;102:8174–8179. [PubMed: 15923262]
37. Baumketner A, Shea J-E. J. Mol. Biol 2006;362:567–579. [PubMed: 16930617]
38. Baumketner A, Shea J-E. J. Mol. Biol 2007;366:275–285. [PubMed: 17166516]
39. Zheng W, Andrec M, Gallicchio E, Levy RM. Proc. Natl. Acad. Sci. USA 2007;104:15340–15345. [PubMed: 17878309]
40. Kabsch W, Sander C. Biopolymers 1983;22:2577–2637. [PubMed: 6667333]
41. Munoz V, Serrano L. Proteins: Struct. Funct. Genet 1994;20:301–311. [PubMed: 7731949]
42. Street AG, Mayo SL. Proc. Natl. Acad. Sci. USA 1999;96:9074–9076. [PubMed: 10430897]
43. Frishman D, Argos P. Proteins Struct. Funct. Gen 1995;23:566–579.
44. Ferrenberg AM, Swendsen RH. Phys. Rev. Lett 1989;63:1195–1198. [PubMed: 10040500]
45. Klimov DK, Thirumalai D. Chem. Phys 2004;307:251–258.
46. Xu XP, Case DA. J. Biomol. NMR 2001;21:321–333. [PubMed: 11824752]
47. Hou L, Shao H, Zhang Y, Li H, Menon NK, Neuhaus EB, Brewer JM, Byeon I-JL, Ray DG, Vitek MP, Iwashita T, Makula RA, Przybyla AB, Zagorski MG. J. Amer. Chem. Soc 2004;126:1992–2005. [PubMed: 14971932]
48. Wang Y, Jardetzky O. Prot. Sci 2002;11:852–861.
49. Cecchini M, Curcio R, Pappalardo M, Melki R, Caflisch A. J. Mol. Biol 2006;357:1306–1321. [PubMed: 16483608]
50. Melquiond A, Dong X, Mousseau N, Derreumaux P. Curr. Alzh. Res 2008;5:244–250.
51. Luhrs T, Ritter C, Adrian M, Loher B, Bohrmann DR, Dobeli H, Schubert D, Riek R. Proc. Natl. Acad. Sci. USA 2005;102:17342–17347. [PubMed: 16293696]
52. Meinhardt J, Tartaglia GG, Pawar A, Christopeid T, Hortschansky P, Schroeckh V, Dobson CM, Vendruscolo M, Fandrich M. Prot. Sci 2007;16:1214–1222.
53. Wu C, Lei H, Duan Y. J. Amer. Chem. Soc 2005;127:13530–13537. [PubMed: 16190716]

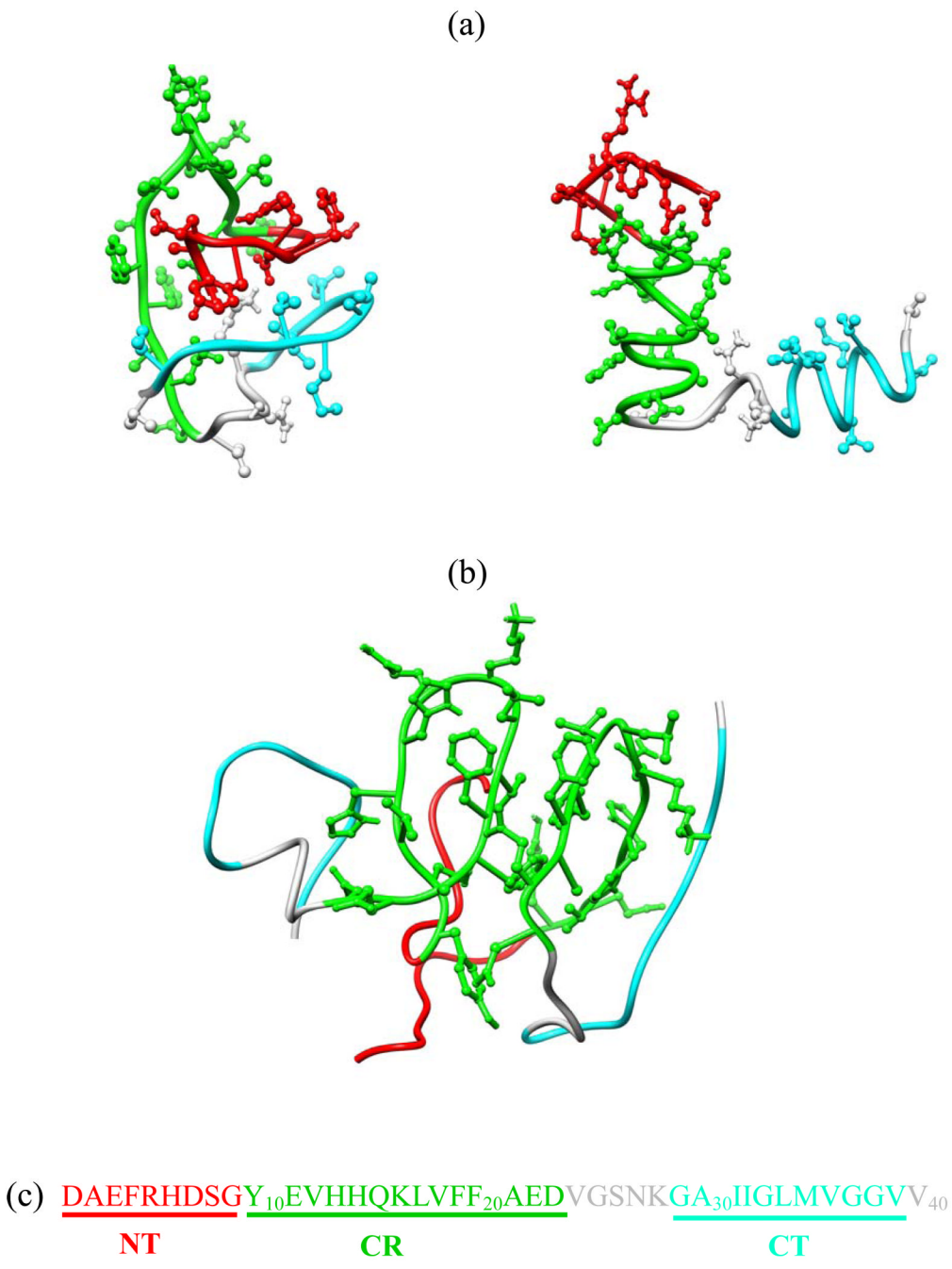

Fig. 1.

Representative snapshots of $A\beta_{1-40}$ (a) monomers and (b) dimers. (c) Sequence of $A\beta_{1-40}$ peptide. NT, CR, and CT regions in (a–c) are in red, green, and aqua, respectively. The turn between the CR and CT and Val40 (which is not part of the second fibril β-strand) are in grey. Two conformers of $A\beta_{1-40}$ monomer are shown, in which NT-CR and NT-CT side chain interactions are formed (left structure) or broken (right structure). Formation of these interactions induces β-structure in the CR and CT, while suppressing helix conformations. In $A\beta_{1-40}$ dimer (b) the aggregation interface predominantly involves the CR and NT regions, leaving the CT regions exposed to solvent.

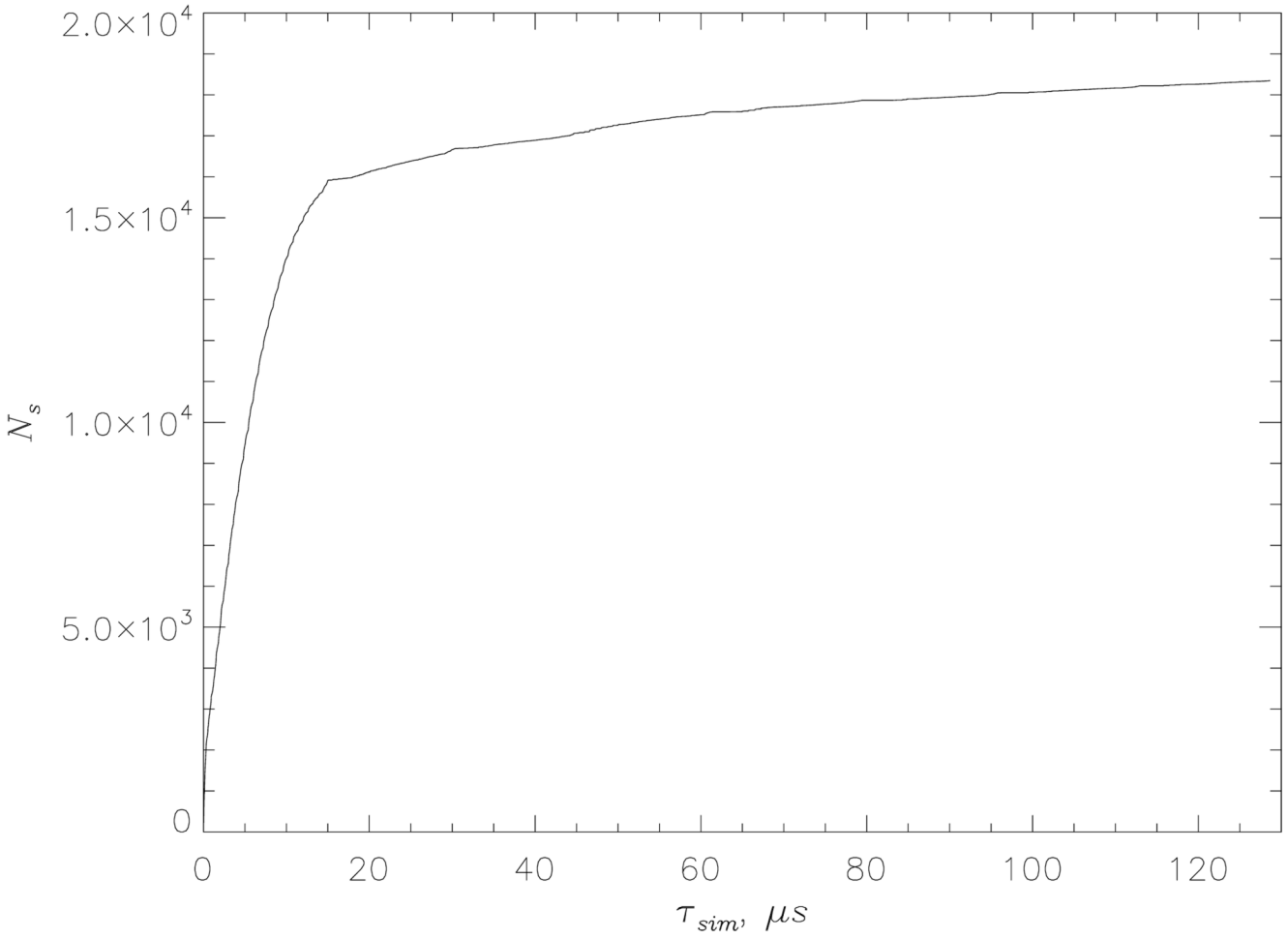

Fig. 2.
The number N_s of the new states (E_{eff}, N_d) in $A\beta_{1–40}$ dimer not previously sampled in REMD as a function of the cumulative equilibrium simulation time τ_{sim}.

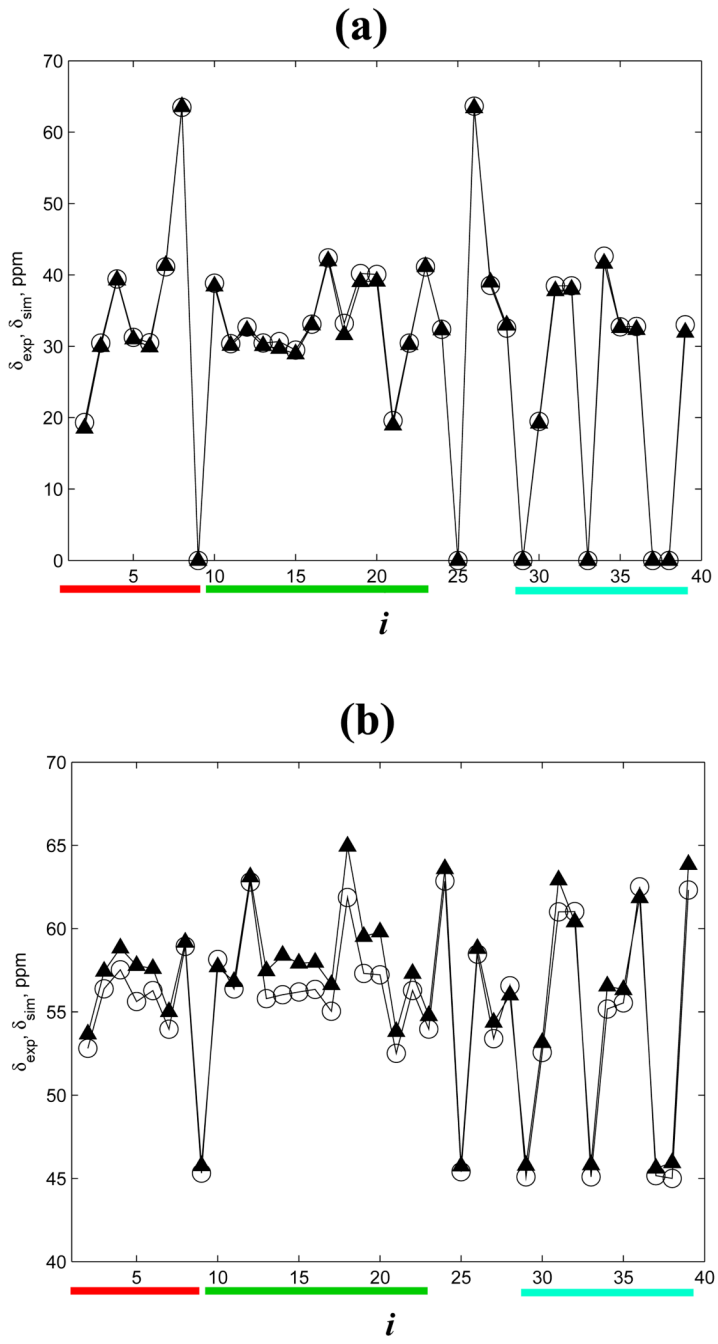

Fig. 3.

Experimental $\delta_{exp}(i)$ (open circles) and simulation $\delta_{sim}(i)$ (triangles) chemical shifts in $A\beta_{1-40}$ monomer as a function of residue number *i:* (a) C_β atoms, (b) C_α atoms. Chemical shifts of Gly C_β atoms are set to zero. The red, green, and aqua bars represent the NT, CR, and CT regions in this figure and in Fig. 4,Fig. 5,Fig. 7.

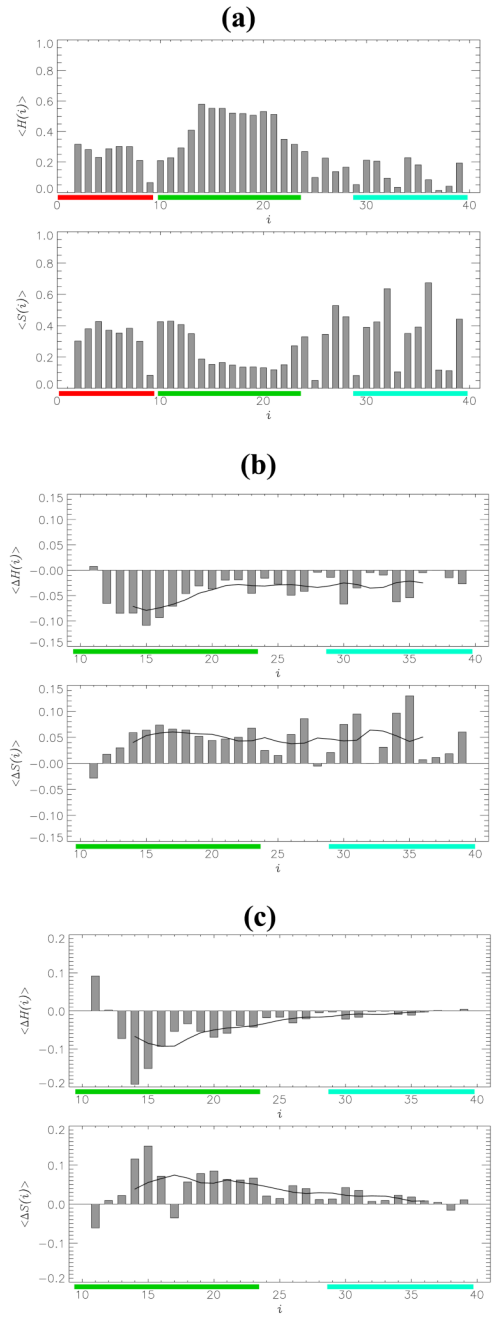

Fig. 4.

(a) Thermal distributions of the fractions of helix < $H(i)$ > and β-strand < $S(i)$ > structures formed by individual residues i in $A\beta_{1–40}$ monomer. The average fraction of β-strand marginally exceeds that of helix states. (b,c) Changes in secondary structure < $\Delta S(i)$ > and < $\Delta H(i)$ > for residues i in $A\beta_{1–40}$ monomer (b) and dimer (c) with respect to $A\beta_{10–40}$ species. Black curves represent the smoothed < $\Delta S(i)$ > and < $\Delta H(i)$ > profiles obtained with the sliding window of seven residues. In the monomer, changes are spread through the sequence, whereas in the dimer they tend to localize within the CR region.

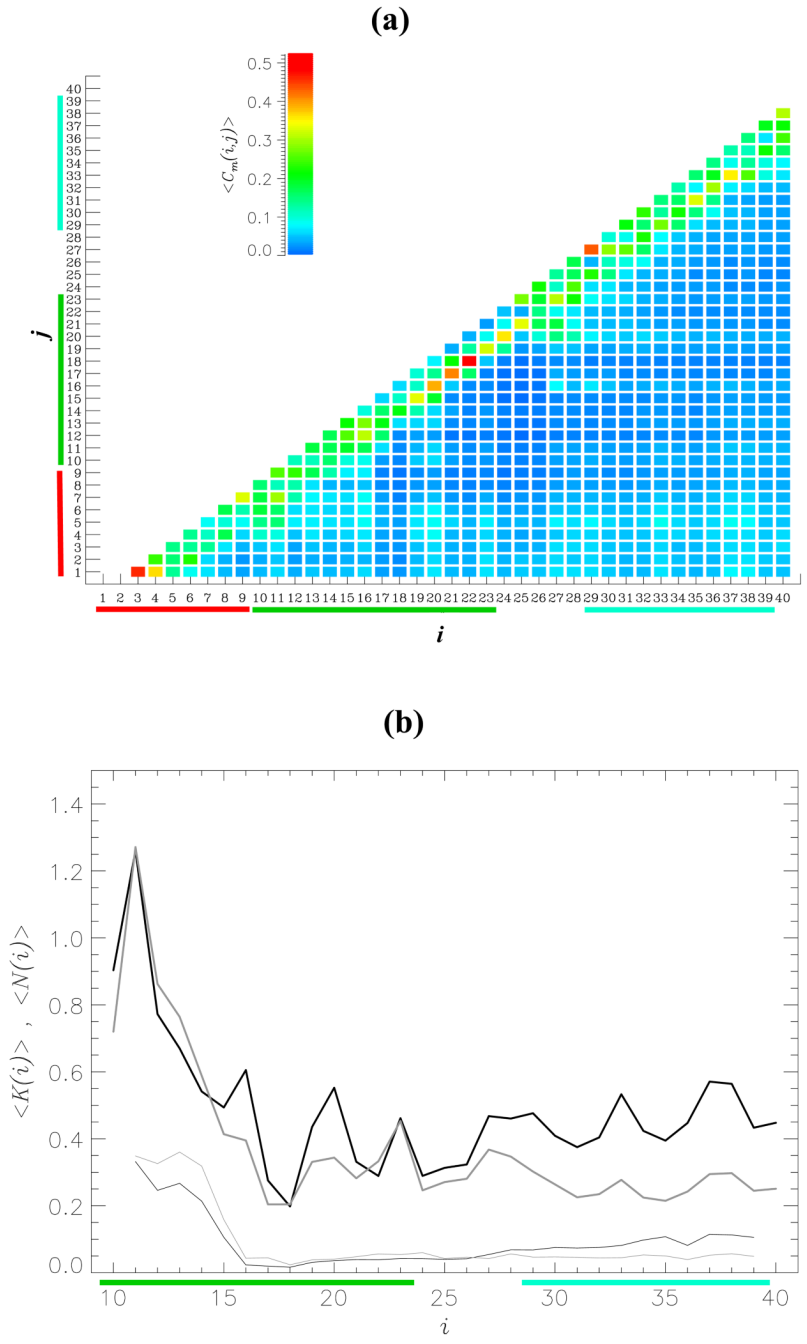

Fig. 5.

(a) The thermal contact map $< C_m(i,j) >$ displays the probabilities of forming side chain contacts between amino acids i and j in $A\beta_{1–40}$ monomer. $< C_m(i, j) >$ is obtained by averaging over the canonical ensemble generated by REMD and is color coded according to the scale shown. The contact map indicates that the NT region forms interactions with the CR and CT regions. (b) The numbers of intrapeptide side chain contacts $< K(i) >$ and HBs $< N(i) >$ formed by the NT with the residues i ($10 \leq i \leq 40$) are shown by thick and thin curves, respectively. The data for monomer and dimer are in black and gray. Compared to side chain contacts the NT region forms few HBs with the rest of $A\beta_{1–40}$ sequence.

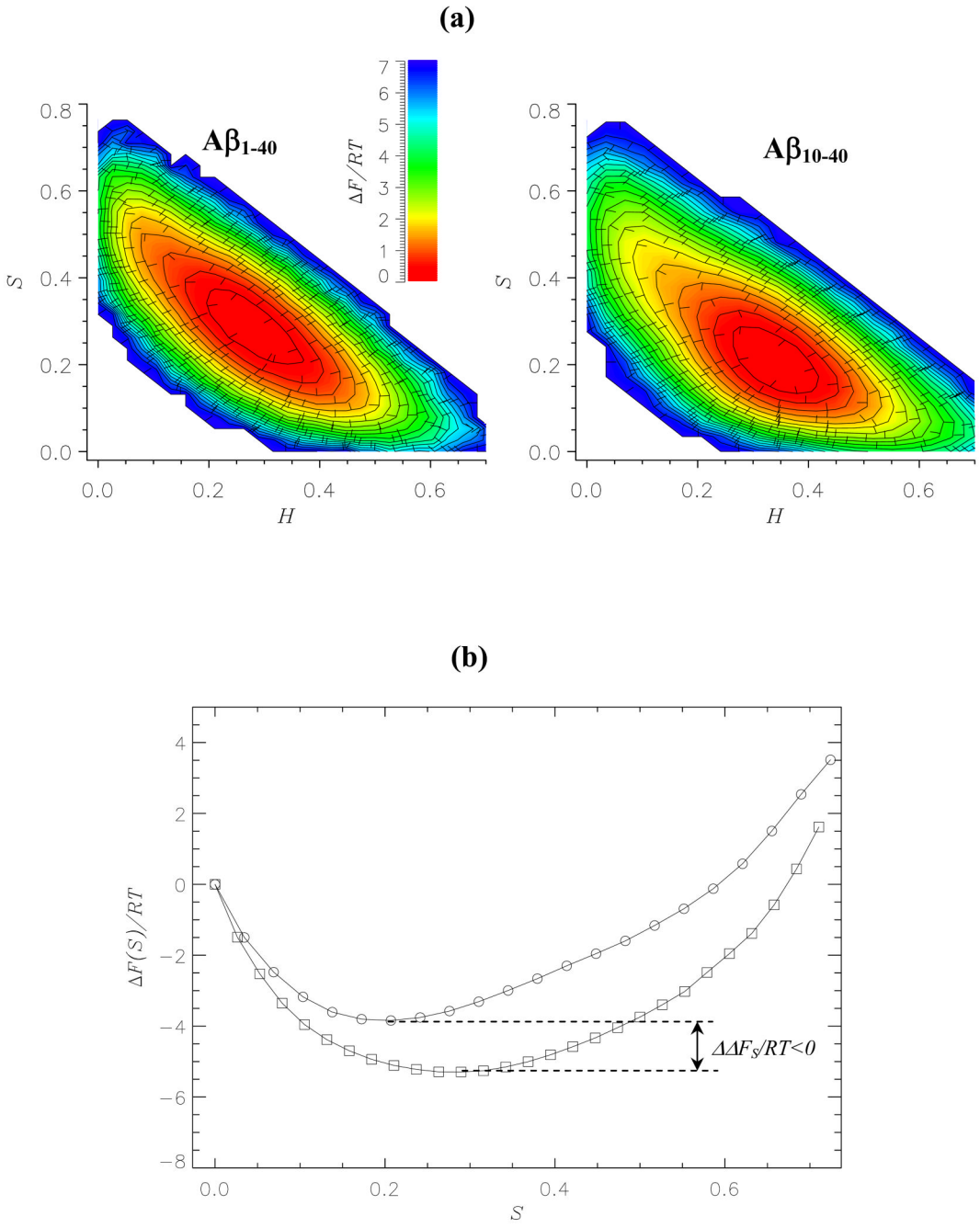

Fig. 6.

(a) Two-dimensional projections of the free energy $\Delta F(H,S)$ as a function of the helix and strand fractions, H and S: $A\beta_{1–40}$ monomer (left panel); $A\beta_{10–40}$ monomer (right panel). The minima in free energy are set to zero. The values of $\Delta F(H, S)$ are color coded according to the scale. (b) One-dimensional profiles of the free energy $\Delta F(S)$: $A\beta_{1–40}$ monomers (squares); $A\beta_{10–40}$ monomers (circles). The states with zero strand contents are set to have zero free energy. The plots in (a) and (b) demonstrate that β-strand structure is stabilized in $A\beta_{1–40}$ compared to $A\beta_{10–40}$. $\Delta\Delta F_S$ is the free energy difference between the β-strand states in $A\beta_{1–40}$ and $A\beta_{10–40}$. β-strand states are operationally defined to have free energies less than $-2RT$.

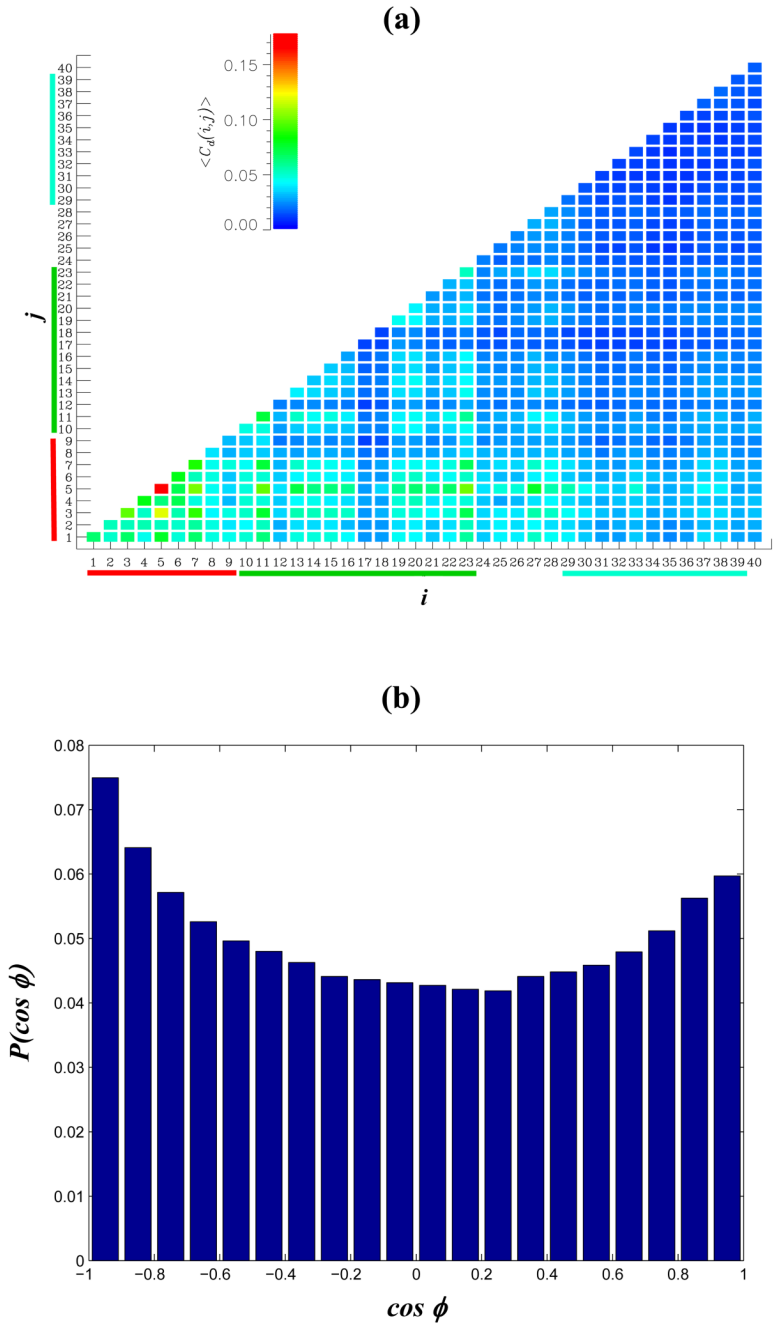

Fig. 7.

(a) The thermal contact map $<C_d(i, j)>$ visualizes the probabilities of forming interpeptide side chain contacts between the residues i and j in $A\beta_{1–40}$ dimer. The aggregation interface in the dimer involves primarily the NT and CR regions, whereas the CT region is weakly engaged in interpeptide interactions. $< C_d(i, j) >$ is color coded according to the scale. (b) The orientation of the CR regions in $A\beta_{1–40}$ dimer is given by the probability distribution $P(cos\phi)$, where ϕ is the angle between the CRs. Antiparallel aggregation interface is weakly preferred.

Table 1

Aggregation interfaces in Aβ dimers[‡] [†]

(a) Numbers of interpeptide side chain contacts < $C_d(s1,s2)$ > in $A\beta_{1-40}$ dimer

	NT	CR	CT
NT	4.7	5.3	3.3
CR		6.2 (0.41)	3.6 (0.24)
CT			1.9 (0.12)

(b) Numbers of interpeptide side chain contacts < $C_d(s1,s2)$ > in $A\beta_{10-40}$ dimer

	CR	CT
CR	8.3 (0.41)	4.8 (0.24)
CT		2.3 (0.11)

[‡] $s1$ and $s2$ denote sequence regions NT, CR, or CT. Due to exhaustive REMD sampling $< C_d(s1,s2) > \approx < C_d(s2,s1) >$.

[†] numbers in parenthesis indicate the fractions of ($s1$,$s2$) contacts computed with respect to the total number of interpeptide contacts formed by the CR and CT regions in the 10–40 fragment of the dimer.

Table 2

Structural clusters of $A\beta_{1–40}$ monomer

(a) Interactions between the NT and CR regions‡

cluster	*p*†	*K*(*NT* – *CR*)	*H*(*CR*)	*S*(*CR*)
CL1	0.31	8.0	0.41	0.27
CL2	0.18	7.4	0.46	0.22
CL3	0.19	7.0	0.53	0.12
CL4	0.12	6.7	0.54	0.13

(b) Interactions between the NT and CT regions‡

cluster	*p*†	*K*(*NT* – *CT*)	*H*(*CT*)	*S*(*CT*)	R_g, Å
CL1	0.19	5.8	0.10	0.37	14.3
CL2	0.31	5.4	0.10	0.38	14.1
CL3	0.12	4.2	0.14	0.33	15.0
CL4	0.18	3.0	0.20	0.18	15.4

‡although both tables list the same cluster distribution, the clusters are relabeled according to the changes in *K*(*NT* – *CR*) in (a) and in *K*(*NT* – *CT*) in (b)

†the fraction of structures included in the cluster